Relativistic properties and invariants of the Du Fort–Frankel scheme for the one-dimensional Schrödinger equation

Paul J. Dellar

OCIAM, Mathematical Institute, University of Oxford, Radcliffe Observatory Quarter, Oxford OX2 6GG, UK

Abstract

The Du Fort–Frankel scheme for the one-dimensional Schrödinger equation is shown to be equivalent, under a time-dependent unitary transformation, to the Ablowitz–Kruskal–Ladik scheme for the Klein–Gordon equation. The Schrödinger equation describes a non-relativistic quantum particle, while the Klein–Gordon equation describes a relativistic particle. The conditional convergence of the Du Fort–Frankel scheme to solutions of the Schrödinger equation arises because solutions of the Klein–Gordon equation only approximate solutions of the Schrödinger equation in the non-relativistic limit. The time-dependent unitary transformation is the discrete analog of the transformation that arises from seeking a non-relativistic limit using the interaction picture of quantum mechanics to decompose the Klein–Gordon Hamiltonian into the relativistic rest energy and a remainder. The Ablowitz–Kruskal–Ladik scheme is in turn decomposed into a quantum lattice gas automaton for the one-dimensional Dirac equation, which is also the one-dimensional discrete time quantum walk. This relativistic interpretation clarifies the origin of the known discrete invariant of the Du Fort–Frankel scheme as expressing conservation of probability for the 2-component wavefunction in the one-dimensional Dirac equation under discrete unitary evolution. It also leads to a second invariant, the matrix element of the evolution operator, whose imaginary part gives a discrete approximation to the expectation of the non-relativistic Schrödinger Hamiltonian.

Key words: discrete invariants; non-relativistic limits; unitary equivalence; lattice algorithms

Journal of Computational Physics: X 2C (2019) 100004 doi:10.1016/j.jcpx.2019.100004

Submitted 15 May 2018, revised 23 December 2018, accepted 24 December 2018, available online 27 February 2019

1. Introduction

The Schrödinger equation for a particle of mass m in a potential V is

$$i\hbar\partial_t\psi = -\frac{\hbar^2}{2m}\nabla^2\psi + V(\mathbf{x})\psi, \tag{1}$$

where $\hbar$ is the reduced Planck's constant [1–3]. This equation describes the evolution of a wavefunction $\psi(\mathbf{x}, t)$, with the interpretation that $|\psi(\mathbf{x}, t)|^2$ is the probability density for the particle to be located at position $\mathbf{x}$ at time t.

More generally, an abstract Schrödinger equation takes the form

$$i\hbar\partial_t\psi = \mathcal{H}\psi, \tag{2}$$

where $\mathcal{H}$ is a self-adjoint linear operator with no explicit time dependence that acts on ψ. The solution of (2) may be written formally as

$$\psi(\cdot, t) = \exp(-i(t/\hbar)\mathcal{H})\psi(\cdot, 0). \tag{3}$$

The evolution is unitary, since $\exp(-i(t/\hbar)t\mathcal{H})$ is a unitary operator because $\mathcal{H}$ is self-adjoint, and time-reversible since $\exp(i(t/\hbar)\mathcal{H})$ is the inverse of $\exp(-i(t/\hbar)\mathcal{H})$. It thus preserves the total probability $\|\psi\|^2 = \int |\psi(\mathbf{x}, t)|^2 d^3x$ (the evolution being unitary restricts the boundary conditions to be consistent with this conservation property). A good numerical scheme for a Schrödinger equation should also generate unitary and time-reversible evolution, but in discrete time steps Δt. In particular, unitary evolution implies stability in the ℓ^2 norm.

The leapfrog or second order difference scheme is [4–9]

$$i\hbar\frac{\psi_j^{n+1} - \psi_j^{n-1}}{2\Delta t} = [\mathsf{H}\psi]_j^n. \tag{4}$$

The wavefunction ψ for a particle moving in one dimension can be approximated by its values $\psi_j^n = \psi(j\Delta x, n\Delta t)$ on a discrete spatial grid indexed by j at discrete times $t = n\Delta t$ indexed by n. A natural discrete Hamiltonian matrix H for

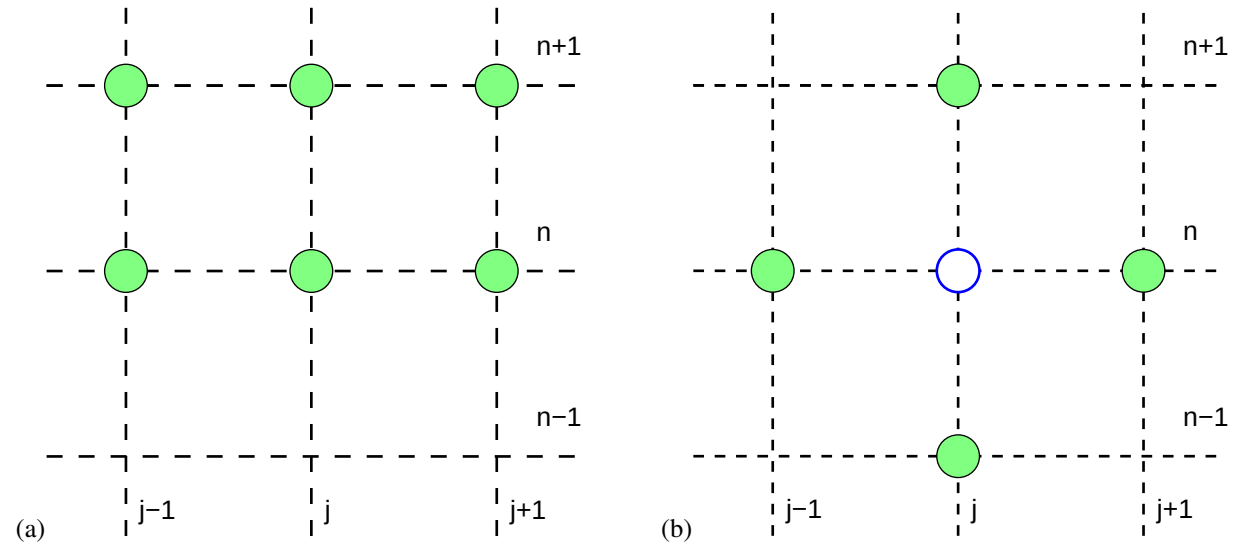

Figure 1: (a) The six-point stencil for the Crank–Nicolson scheme across the two time levels n and $n+1$. (b) The four-point stencil for the Du Fort–Frankel scheme across the three time levels $n-1$, n, and $n+1$. The central point (open circle) is only required for the five-point leapfrog, Harmuth and Perring–Skyrme schemes described in the appendix.

a free particle (one with $V = 0$) is defined by discretising the Laplacian in (1) using the 3-point centred finite difference approximation

$$[\mathsf{H}\psi]_j^n = -\frac{\hbar^2}{2m}\frac{1}{\Delta x^2}\left(\psi_{j+1}^n - 2\psi_j^n + \psi_{j-1}^n\right), \tag{5}$$

so the abstract leapfrog scheme (4) becomes

$$i\hbar\frac{\psi_j^{n+1} - \psi_j^{n-1}}{2\Delta t} = -\frac{\hbar^2}{2m}\left(\frac{\psi_{j+1}^n - 2\psi_j^n + \psi_{j-1}^n}{\Delta x^2}\right). \tag{6}$$

This paper is primarily concerned with the Du Fort–Frankel scheme introduced by Wu [10]

$$i\hbar\frac{\psi_j^{n+1} - \psi_j^{n-1}}{2\Delta t} = -\frac{\hbar^2}{2m}\left(\frac{\psi_{j+1}^n - \left(\psi_j^{n+1} + \psi_j^{n-1}\right) + \psi_{j-1}^n}{\Delta x^2}\right). \tag{7}$$

This scheme is obtained by replacing $2\psi_j^n$ in (6) with the average $\left(\psi_j^{n+1} + \psi_j^{n-1}\right)$, the same replacement made by Du Fort & Frankel to construct their scheme for the real diffusion equation [11]. The scheme thus uses the four-point stencil shown in Fig. 1(b). It omits ψ_j^n located at the central point of the stencil. The Du Fort–Frankel scheme (7) is unconditionally stable, unlike the leapfrog scheme (6), and one can rearrange (7) to give an explicit formula for ψ_j^{n+1} locally at each grid point (see section 3).

These properties make the Du Fort–Frankel scheme an attractive alternative to the Crank–Nicholson scheme. The latter uses the Cayley transform [12]

$$\left(\mathsf{I} + \tfrac{1}{2}i(\Delta t/\hbar)\mathsf{H}\right)^{-1}\left(\mathsf{I} - \tfrac{1}{2}i(\Delta t/\hbar)\mathsf{H}\right) \tag{8}$$

to construct a unitary and time-reversible approximation to $\exp(-i\Delta t\mathsf{H}/\hbar)$ for the evolution between two time levels, given concretely by

$$i\hbar\frac{\psi_j^{n+1} - \psi_j^n}{\Delta t} = -\frac{\hbar^2}{2m}\frac{1}{2}\left(\frac{\psi_{j+1}^{n+1} - 2\psi_j^{n+1} + \psi_{j-1}^{n+1}}{\Delta x^2} + \frac{\psi_{j+1}^n - 2\psi_j^n + \psi_{j-1}^n}{\Delta x^2}\right). \tag{9}$$

This scheme uses the six point stencil shown in Fig. 1(a). It is implicit, because each timestep requires the solution of a tridiagonal linear system involving the operator $\left(\mathsf{I} + \frac{1}{2}i(\Delta t/\hbar)\mathsf{H}\right)$ to determine the ψ_j^{n+1} at all grid points j. This complicates a parallel implementation. The widely used Thomas algorithm for solving tridiagonal systems is inherently serial, though parallel alternatives, such as cyclic reduction or diagonalisation by discrete Fourier transform, are available. The implicitness incurs significantly more computational complexity and expense in multiple spatial dimensions, as some iterative algorithm will typically be required to solve the linear system. Like the above Du Fort–Frankel scheme, this is the complex version of the Crank–Nicolson [13] scheme for the real diffusion equation.

The Schrödinger equation (1) contains one time derivative but two spatial derivatives. The same asymmetry appears in the stencil for the Crank–Nicholson scheme, which contains three spatial points at each of two time levels. This asymmetry between space and time makes the Schrödinger equation incompatible with special relativity, which requires an equation to be invariant under Lorentz transformations that mix the space and time coordinates.

By contrast, space and time appear symmetrically in the four-point stencil for the Du Fort–Frankel scheme shown in Fig. 1(b). This paper will explore the properties of the Du Fort–Frankel scheme as a discretisation of a *relativistic* quantum wave equation, not of the Schrödinger equation (1).

2. Relativistic wave equations

The Schrödinger equation (1) for a free particle coincides with the Newtonian expression $E = |\mathbf{p}|^2/(2m)$ for the energy of a free classical point particle with momentum $\mathbf{p}$ and mass m when one replaces E and $\mathbf{p}$ by differential operators:

$$E \to i\hbar\partial_t, \quad \mathbf{p} \to -i\hbar\nabla. \tag{10}$$

Making the same replacements in the relativistic energy-momentum relation $E^2 = c^2|\mathbf{p}|^2 + m^2c^4$ for a free classical point particle gives the Klein–Gordon equation [1–3]

$$\partial_{tt}u - c^2\nabla^2 u = -(mc^2/\hbar)^2 u. \tag{11}$$

The line element $ds^2 = |d\mathbf{x}|^2 - c^2dt^2$, and hence the differential operator $\partial_{tt} - c^2\nabla^2$ on the left hand side, are invariant under Lorentz transformations. The whole equation is thus Lorentz-invariant if we treat u as a Lorentz-invariant scalar field.

By construction, the Klein–Gordon equation has plane wave solutions proportional to $\exp(i(\mathbf{k}\cdot\mathbf{x} - \omega t))$ that satisfy the dispersion relation

$$\omega^2 = c^2|\mathbf{k}|^2 + (mc^2/\hbar)^2. \tag{12}$$

This is just a rewriting of the above energy-momentum relation using the frequency $\omega = E/\hbar$ and wave vector $\mathbf{k} = \mathbf{p}/\hbar$. Unlike the previous Schrödinger equation, there are two branches of solutions: one with positive frequencies $\omega \geq mc^2/\hbar$, and one with negative frequencies $\omega \leq -mc^2/\hbar$. Expanding the positive branch for $|\mathbf{k}| \ll mc/\hbar$ gives

$$\omega = c\sqrt{(mc/\hbar)^2 + |\mathbf{k}|^2} = mc^2/\hbar + \hbar|\mathbf{k}|^2/(2m) + O(|\mathbf{k}|^4). \tag{13}$$

This recovers the dispersion relation $\omega = \hbar|\mathbf{k}|^2/(2m)$ for the Schrödinger equation, but offset by the Compton frequency $mc^2/\hbar$ associated with the relativistic rest energy mc^2. The group velocity for both signs of ω is

$$\nabla_{\mathbf{k}}\omega = (c^2/\omega)\mathbf{k}. \tag{14}$$

This satisfies the bound $|\nabla_{\mathbf{k}}\omega| < c$, and coincides with the expression

$$\mathbf{v} = \frac{\mathbf{p}}{\sqrt{m^2 + |\mathbf{p}|^2/c^2}} \tag{15}$$

for the velocity $\mathbf{v}$ of a relativistic particle with momentum $\mathbf{p}$.

The fundamental solution of the one-dimensional Klein–Gordon equation for a concentrated Dirac δ-function source at (ξ, τ) is [14]

$$u(x,t) = \begin{cases} J_0\left(m\sqrt{(t-\tau)^2 - (x-\xi)^2/c^2}\right)/(2c), & \text{for } |x-\xi| \leq c|t-\tau|, \\ 0, & \text{for } |x-\xi| > c|t-\tau|, \end{cases} \tag{16}$$

where J_0 is the Bessel function of the first kind of order zero. The support of this solution is thus confined to the boundary and interior of the light cone $|x - \xi| = c|t - \tau|$, as one would expect from the bound on the group velocity. However, the support occupies the whole interior of the light cone, rather than being confined to the light cone itself, as for the corresponding fundamental solution of the wave equation. By contrast, the support of the fundamental solution

$$\psi(x,t) = (2\pi i\, t\hbar/m)^{-1/2} \exp\left(i\, x^2/(2t\hbar/m)\right) \tag{17}$$

of the one-dimensional Schrödinger equation extends over the whole domain.

The Schrödinger equation (1) implies an equation for conservation of probability,

$$\partial_t\left(|\psi|^2\right) + \nabla\cdot\left(\frac{i\hbar}{2m}\left(\psi\nabla\overline{\psi} - \overline{\psi}\nabla\psi\right)\right) = 0, \tag{18}$$

with a flux called the probability current [1–3]. An overbar denotes a complex conjugate. The Klein–Gordon equation (11) implies another conservation law with the same flux:

$$\partial_t\left(\frac{i\hbar}{2mc^2}\left(\overline{u}\partial_t u - u\partial_t\overline{u}\right)\right) + \nabla\cdot\left(\frac{i\hbar}{2m}\left(u\nabla\overline{u} - \overline{u}\nabla u\right)\right) = 0. \tag{19}$$

However, the quantity appearing in the time derivative cannot be interpreted as a probability density. It is not positive definite, as we can specify u and u_t independently as initial conditions for the second-order Klein–Gordon equation.

2.1. Dirac equation

This difficulty led Dirac to seek a relativistic wave equation involving only first derivatives in space and time. This also fits the abstract Schrödinger equation (2) that generates evolution through the unitary operator $\exp(-it\mathcal{H}/\hbar)$. In one spatial dimension this is accomplished by the system

$$\partial_t u + c\partial_z u = (mc^2/\hbar)d, \tag{20a}$$
$$\partial_t d - c\partial_z d = -(mc^2/\hbar)u, \tag{20b}$$

which takes the form (2) with the matrix Hamiltonian

$$\mathcal{H} = \begin{pmatrix} -ic\hbar\partial_z & imc^2 \\ -imc^2 & ic\hbar\partial_z \end{pmatrix} \tag{21}$$

acting on the 2-component wavefunction $\Phi_2 = (u, d)^\mathsf{T}$. Eliminating d between these two equations leads back to the Klein–Gordon equation (see Section 6). The left hand sides of (20) describe the propagation of u and d along characteristics with speeds $\pm c$, as appropriate for a massless particle. The mass terms on the right hand sides mix these two propagation directions, leading to the characteristic "Zitterbewegung" or trembling motion of a relativistic particle [1–3].

This factorisation of the one-dimensional Klein–Gordon equation into a first-order system with the self-adjoint Hamiltonian (21) relies on the factorisation $\partial_{tt} - c^2\partial_{zz} = (\partial_t + c\partial_z)(\partial_t - c\partial_z)$. More generally, the three-dimensional Dirac equation requires a 4-component wavefunction Φ_4, and factorises the three-dimensional Laplacian as $(\boldsymbol{\sigma}\cdot\nabla)^2 = \mathsf{I}_2\nabla^2$, where I_2 is the 2×2 identity matrix, using the three Pauli spin matrices [1–3]

$$\sigma_x = \begin{pmatrix} 0 & 1 \\ 1 & 0 \end{pmatrix}, \quad \sigma_y = \begin{pmatrix} 0 & -i \\ i & 0 \end{pmatrix}, \quad \sigma_z = \begin{pmatrix} 1 & 0 \\ 0 & -1 \end{pmatrix}. \tag{22}$$

The three-dimensional Dirac equation reduces to two independent copies of the system (20) for wavefunctions that depend only on z and t. It is convenient to choose z as the spatial coordinate because σ_z is diagonal.

More generally, given a wavefunction that solves the Dirac equation, every component individually solves the Klein–Gordon equation (which just expresses the relativistic energy-momentum relation). However, the extra structure in the Dirac equation as a first order system changes the interpretation of the solution. In particular, the system (20a,b) implies a conservation law for the positive-definite probability density $|u|^2 + |d|^2$,

$$\partial_t\left(|u|^2 + |d|^2\right) + \nabla\cdot\left(c(|u|^2 - |d|^2)\right) = 0. \tag{23}$$

2.2. Interaction picture and non-relativistic limit

The abstract Schrödinger equation (2) describes the evolution of the wavefunction ψ in time. Physically meaningful quantities are expressed as expectations of self-adjoint linear operators $\mathcal{A}$, known as observables, defined by

$$\mathbb{E}(\mathcal{A}) = \frac{\langle\mathcal{A}\rangle}{\|\psi\|^2}, \quad \text{where } \langle\mathcal{A}\rangle = \int \overline{\psi}\mathcal{A}\psi\, d^3x, \text{ and } \|\psi\|^2 = \int |\psi|^2\, d^3x. \tag{24}$$

The expectation is invariant under global changes of phase: $\psi \mapsto \psi e^{i\alpha}$ for any constant α.

The operators $\mathcal{A}$ usually have no explicit time dependence. For example, the probability of the particle described by the concrete Schrödinger equation (1) being in some subset X of space is given by taking $\mathcal{A}$ to be the indicator function for $x \in X$. It is common to normalise the wavefunction so that $\|\psi\| = 1$. The expectation $\mathbb{E}(\mathcal{A})$ then coincides with the matrix element $\langle\mathcal{A}\rangle$. However, the recovery of the expectation of the Hamiltonian for the Schrödinger equation in the non-relativistic limit depends crucially on the different normalisations of the relativistic and non-relativistic theories.

This Schrödinger picture is just one approach to formulating quantum mechanics. The interaction, or Dirac, picture decomposes the Hamiltonian into $\mathcal{H} = \mathcal{H}_0 + \mathcal{H}_I$. If ϕ is the wavefunction in the Schrödinger picture that satisfies $i\hbar\partial_t\phi = (\mathcal{H}_0 + \mathcal{H}_I)\phi$, the wavefunction

$$\psi(x,t) = e^{i\mathcal{H}_0 t/\hbar}\phi(x,t), \tag{25}$$

in the interaction picture evolves according to [3]

$$i\hbar\partial_t\psi = e^{i\mathcal{H}_0 t/\hbar}\mathcal{H}_I e^{-i\mathcal{H}_0 t/\hbar}\psi. \tag{26}$$

We use ψ for the transformed wavefunction so that we later obtain the familiar non-relativistic Schrödinger equation for ψ by applying the interaction picture to a relativistic wave equation for ϕ.

More generally, any time-independent operator $\mathcal{A}$ in the Schrödinger picture (other than the Hamiltonian) becomes

$$\mathcal{A}_I(t) = e^{i\mathcal{H}_0 t/\hbar}\mathcal{A}e^{-i\mathcal{H}_0 t/\hbar} \tag{27}$$

in the interaction picture. The interaction picture thus interpolates between the Schrödinger picture, for which $\mathcal{H}_0 = 0$, and the Heisenberg picture, for which $\mathcal{H}_0 = \mathcal{H}$ and $\mathcal{H}_I = 0$. The interaction picture is commonly used to construct the wavefunction ϕ using a convergent sequence of nested integrals when $\mathcal{H}_I$ is treated as a perturbation to $\mathcal{H}_0$ [3].

To apply the interaction picture to constructing the non-relativistic limit of the one-dimensional Dirac equation above, we diagonalise the algebraic mass terms $mc^2/\hbar$ in the Hamiltonian (21) by applying the unitary transformation

$$\begin{pmatrix} u \\ d \end{pmatrix} = \frac{1}{\sqrt{2}} \begin{pmatrix} 1 & 1 \\ -i & i \end{pmatrix} \begin{pmatrix} \phi_+ \\ \phi_- \end{pmatrix}. \tag{28}$$

The Hamiltonian becomes

$$\underbrace{\begin{pmatrix} mc^2 & -ic\hbar\partial_z \\ -ic\hbar\partial_z & -mc^2 \end{pmatrix}}_{\mathcal{H}} = \underbrace{\begin{pmatrix} mc^2 & 0 \\ 0 & mc^2 \end{pmatrix}}_{\mathcal{H}_0} + \underbrace{\begin{pmatrix} 0 & -ic\hbar\partial_z \\ -ic\hbar\partial_z & -2mc^2 \end{pmatrix}}_{\mathcal{H}_I}. \tag{29}$$

We thus isolate the rest mass Hamiltonian $\mathcal{H}_0 = mc^2 \mathsf{I}_2$ and treat $\mathcal{H}_I = \mathcal{H} - \mathcal{H}_0$ as a perturbation. As $\mathcal{H}_0$ is a multiple of the identity matrix I_2 it commutes with any other operator $\mathcal{A}$, so $\mathcal{A}_I(t) = \mathcal{A}$ is unchanged according to the prescription (27).

Following (25) we introduce

$$\psi_\pm(\mathbf{x}, t) = \phi_\pm(\mathbf{x}, t) e^{imc^2 t/\hbar}. \tag{30}$$

We will find below that, although $\mathcal{H}_I$ is not small relative to $\mathcal{H}_0$ in the operator norm, $\|\mathcal{H}_I\Psi\|$ is much smaller than $\|\mathcal{H}_0\Psi\|$ for wavefunctions $\Psi = (\psi_+, \psi_-)^\mathsf{T}$ describing non-relativistic solutions. The wavefunctions $\psi_\pm$ evolve according to

$$\partial_t \psi_+ + c\partial_z \psi_- = 0, \tag{31a}$$

$$\partial_t \psi_- + c\partial_z \psi_+ = 2i\frac{mc^2}{\hbar}\psi_-. \tag{31b}$$

The algebraic right hand side now only affects ψ_-. The slowly-varying approximation

$$|\partial_t \psi_-| \ll 2\frac{mc^2}{\hbar}\,|\psi_-|\,, \tag{32}$$

holds in the non-relativistic limit, when the wavefunction oscillates with frequencies much smaller than the Compton frequency $mc^2/\hbar$. Making this approximation in (31b) allows us to solve for ψ_- in terms of the gradient of ψ_+,

$$\psi_- = -\frac{\hbar}{2mc} i\partial_z \psi_+. \tag{33}$$

From this relation we can estimate $|\psi_-|/|\psi_+| \sim |\mathbf{p}|/(2mc)$. The estimate is exact for plane wave solutions, which are eigenfunctions of the momentum operator $\mathbf{p}$. The ratio of the momentum $\mathbf{p}$ to the momentum scale mc is small for a particle moving non-relativistically.

Substituting the relation (33) into the evolution equation (31a) for ψ_+ leads to the one-dimensional Schrödinger equation for a free particle:

$$i\hbar\partial_t \psi_+ = -\frac{\hbar^2}{2m}\partial_{zz}\psi_+. \tag{34}$$

As in derivations of the Navier–Stokes equations from kinetic theory, this derivation of the Schrödinger equation eliminates the fast variable ψ_- to obtain a closed evolution equation for the slow variable ψ_+ alone [15, 16]. The same idea is used in geophysical fluid dynamics to construct balanced models, such as the quasigeostrophic equations. These describe low-frequency motions in rapidly rotating fluid flows, while eliminating high-frequency inertia-gravity waves, by formulating a closed evolution equation for the height or potential vorticity field alone [17].

The matrix element of the interaction Hamiltonian is

$$\langle \mathcal{H}_I \rangle = \int -2mc^2|\psi_-|^2 - ic\hbar\left(\overline{\psi_+}\partial_z\psi_- + \overline{\psi_-}\partial_z\psi_+\right) dz. \tag{35}$$

If we insert the approximation (33) for ψ_- in terms of ψ_+, $\langle \mathcal{H}_I \rangle$ coincides with the matrix element of the Schrödinger Hamiltonian for the ψ_+ state,

$$\langle \mathcal{H}_S \rangle = \int -\frac{1}{2m}\overline{\psi_+}\partial_{zz}\psi_+ dz = \int \frac{1}{2m}|\partial_z\psi_+|^2 dz. \tag{36}$$

The second step requires the usual integration by parts. Another useful expression, when ψ_+ and ψ_- are related by (33), is

$$\langle \mathcal{H}_I \rangle = \int 2mc^2|\psi_-|^2 dz, \tag{37}$$

which is also equal to $\langle \mathcal{H}_S \rangle$. However, the natural normalisation of the 2-component wavefunction for the interaction picture of the Klein–Gordon equation differs from the normalisation of the Schrödinger equation. The expectations of $\mathcal{H}_I$ and $\mathcal{H}_S$ are

$$\mathbb{E}(\mathcal{H}_S) = \frac{\langle \mathcal{H}_S \rangle}{\|\psi_+\|^2}, \quad \mathbb{E}(\mathcal{H}_I) = \frac{\langle \mathcal{H}_I \rangle}{\|\psi_+\|^2 + \|\psi_-\|^2}. \tag{38}$$

Only the sum $\|\psi\|^2 = \|\psi_+\|^2 + \|\psi_-\|^2$ is conserved by the Klein–Gordon equation. Neither term is conserved separately. However, we can use (37) to replace $\|\psi_-\|^2$ by $\langle \mathcal{H}_I \rangle/(2mc^2)$ in the non-relativistic limit, which implies

$$\mathbb{E}(\mathcal{H}_S) = \left(1 + \frac{\|\psi_-\|^2}{\|\psi_+\|^2}\right)\mathbb{E}(\mathcal{H}_I) = \frac{\langle \mathcal{H}_I \rangle}{\|\psi\|^2 - \langle \mathcal{H}_I \rangle/(2mc^2)}. \tag{39}$$

We can thus recover the expectation of the Hamiltonian in the Schrödinger equation from the invariants $\|\psi\|^2$ and $\langle \mathcal{H}_I \rangle$ of the Klein–Gordon equation in the interaction picture.

The transformation (30) based on the interaction picture is equivalent to the substitution made by Pauli [2] to break the symmetry between ϕ_+ and ϕ_- by seeking solutions whose time-dependence is close to $e^{-imc^2 t/\hbar}$. The same Wentzel–Kramers–Brillouin (WKB)-like ansatz [18]

$$u(\mathbf{x}, t) = \psi(\mathbf{x}, t) e^{imc^2 t/\hbar} \tag{40}$$

transforms the Klein–Gordon equation (11) into the complex telegraph equation

$$-\frac{\hbar^2}{2mc^2}\partial_{tt}\psi + i\hbar\partial_t\psi = -\frac{\hbar^2}{2m}\nabla^2\psi. \tag{41}$$

We can now motivate the Schrödinger equation as describing solutions $\psi(\mathbf{x}, t)$ that vary sufficiently slowly in time, with frequencies much less than the Compton frequency $mc^2/\hbar$, that we can neglect the first term relative to the second term on the left hand side. We can also motivate rewriting the Du Fort–Frankel scheme (7) as a centred finite difference discretisation of the one-dimensional complex telegraph equation:

$$-\frac{\hbar^2}{2mc^2}\frac{\psi_j^{n+1} - 2\psi_j^n + \psi_j^{n-1}}{\Delta t^2} + i\hbar\frac{\psi_j^{n+1} - \psi_j^{n-1}}{2\Delta t} = -\frac{\hbar^2}{2m}\frac{\psi_{j+1}^n - 2\psi_j^n + \psi_{j-1}^n}{\Delta x^2}. \tag{42}$$

This follows Du Fort & Frankel's observation that solutions of their scheme converge to solutions of a real telegraph equation, rather than to solutions of a diffusion equation [11]. The form (42) also leads to a more general class of Du Fort–Frankel schemes in which one takes an existing scheme with a finite difference approximation to a first time derivative $\partial_t\psi$, as illustrated by the second term on the left hand side of (42), and adds a constant multiple of the centred finite difference approximation to $\partial_{tt}\psi$ with a constant chosen to optimise the stability of the overall scheme [19, 20].

The transformation (30) can also be interpreted as a special case of the general invariance of the Schrödinger and Klein–Gordon equations under the gauge transformations

$$\phi(\mathbf{x}, t) = \psi(\mathbf{x}, t) e^{i\chi(\mathbf{x},t)} \tag{43}$$

when appropriate scalar $V = \partial_t\chi$ and vector $\mathbf{A} = \nabla\chi$ potentials are included. This transformation is thus distinct from the earlier transformation under (24) that changed the phase of the wavefunction by a constant. By taking the gauge function χ to be an affine function of t alone, one can absorb the relativistic energy due to the rest mass into a constant scalar potential, leaving the equivalent of the interaction Hamiltonian $\mathcal{H}_I$.

3. Dispersion relations for the Du Fort–Frankel and other schemes

We first rewrite Wu's Du Fort–Frankel scheme (7) as

$$i\left(\psi_j^{n+1} - \psi_j^{n-1}\right) = -\frac{1}{\lambda}\left(\psi_{j+1}^n - \left(\psi_j^{n+1} + \psi_j^{n-1}\right) + \psi_{j-1}^n\right), \tag{44}$$

with a single dimensionless parameter $\lambda = m\Delta x^2/(\hbar\Delta t)$. This becomes $\lambda = (mc^2/\hbar)\Delta t$ on putting $\Delta x = c\Delta t$. Thus λ is the change in phase over a timestep Δt for an oscillation at the Compton frequency $mc^2/\hbar$. From now on it is more convenient to adopt dimensionless, so-called natural, units in which $c = 1$ and $\hbar = 1$, so $\lambda = m\Delta t$.

Equation (44) is formally implicit, since ψ_j^{n+1} appears on both sides, but we can solve locally for

$$\psi_j^{n+1} = -\frac{1 + i\lambda}{1 - i\lambda}\psi_j^{n-1} + \frac{1}{1 - i\lambda}\left(\psi_{j+1}^n + \psi_{j-1}^n\right). \tag{45}$$

There is no need to solve a linear system that couples different grid points, as needed for the Crank–Nicolson scheme (9). Equation (45) may be rewritten more simply as

$$\psi_j^{n+1} = -e^{2i\alpha}\psi_j^{n-1} + \frac{1}{2}\left(1 + e^{2i\alpha}\right)\left(\psi_{j+1}^n + \psi_{j-1}^n\right) \tag{46}$$

by introducing $\alpha = \tan^{-1}\lambda$. Seeking plane wave solutions with $\psi_j^n = \exp(i(kj\Delta x - \omega n\Delta t))$ yields the dispersion relation

$$\cos(\omega\Delta t + \alpha) = \cos(k\Delta x)\cos\alpha. \tag{47}$$

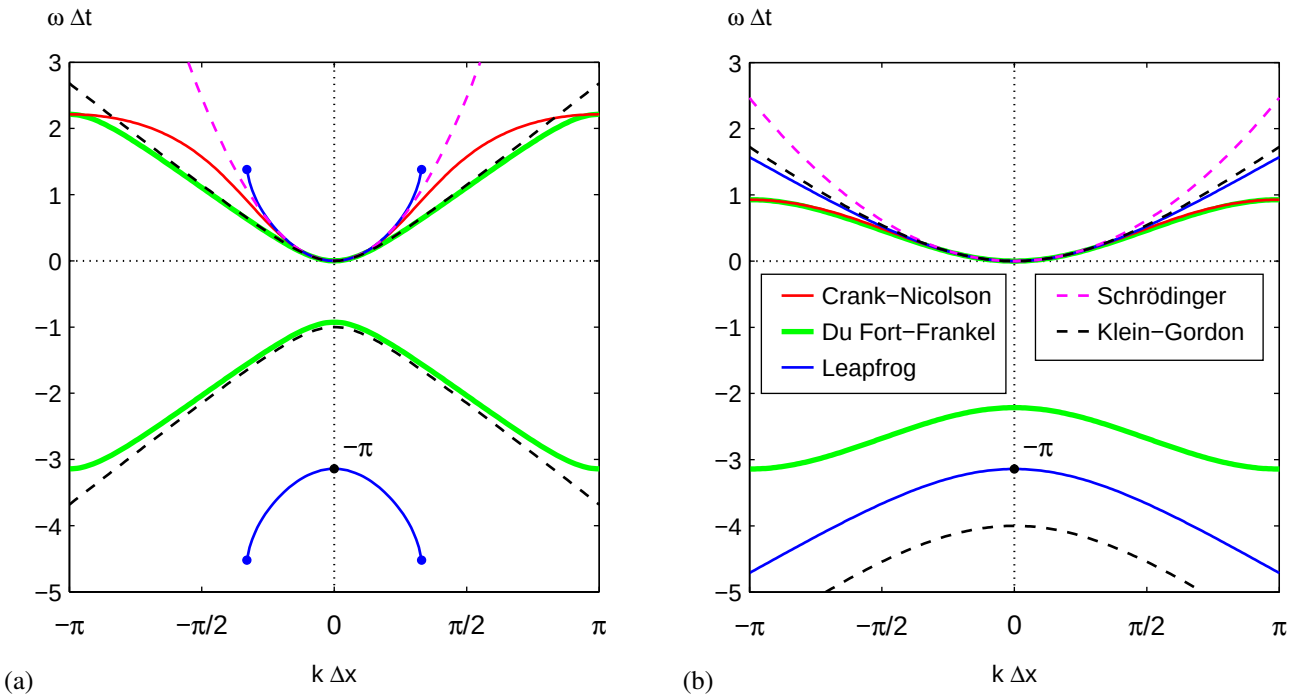

Figure 2: Dispersion relations for the leapfrog, Du Fort–Frankel (DF) and Crank–Nicolson (CN) schemes, and for the Schrödinger and shifted Klein–Gordon equations, for dimensionless mass parameters (a) $\lambda = 1/2$ and (b) $\lambda = 2$. For $\lambda = 2$, the upper branch of the DF dispersion relation almost coincides with the CN dispersion relation. The blue dots mark the ends of the stable region for the LF scheme, whose lower branch passes through $\omega\Delta t = -\pi$ at $k = 0$. The right-hand legend applies to both plots.

There are two real frequencies ω for each k and α, so the scheme is indeed unconditionally stable. The left-hand side is an even function of $\omega\Delta t + \alpha$, and for $k = 0$ the two roots are $\omega = 0$ and $\omega\Delta t = -2\alpha$. For small k there is a branch with $\omega \sim k^2/(2m)$, which agrees with the dispersion relation of the Schrödinger equation.

The dispersion relation for the Crank–Nicolson scheme (9) is

$$\tan(\omega_{CN}\Delta t/2) = \frac{1}{\lambda}\sin^2(k\Delta x/2)\,. \tag{48}$$

This equation always has a solution for a real frequency ω_{CN} for all real k and λ, so this scheme is also unconditionally stable. The dispersion relation for the leapfrog scheme in (6) is

$$\sin(\omega_{LF}\Delta t) = \frac{2}{\lambda}\sin^2(k\Delta x/2)\,. \tag{49}$$

This only has a solution for a real frequency ω_{LF} for all real k when $\lambda \geq 2$, as found by Harmuth [5]. Moreover, there are then two real solutions, one with $\omega_{LF} \to 0$ as $k \to 0$, and a second with $\omega_{LF} \to -\pi/\Delta t$ as $k \to 0$. For the special case $\lambda = 2$, shown in Fig. 2(b), the group velocity $d\omega_{LF}/dk$ is discontinuous at $k = \pm\pi/\Delta x$. For larger λ, the group velocity vanishes at $k = \pm\pi/\Delta x$ for the leapfrog scheme, just as it does for the Du Fort–Frankel and Crank–Nicolson schemes. The dispersion relations for the numerical schemes are all 2π-periodic, unlike the dispersion relations for the partial differential equations (PDEs).

Figure 2 compares the dispersion relations for the Du Fort–Frankel, leapfrog, and Crank–Nicolson schemes, for the two parameter values $\lambda = 1/2$ and $\lambda = 2$, with the dispersion relation of the Schrödinger equation, and with the dispersion relation of the Klein–Gordon equation shifted by $-\lambda$,

$$\omega_{KG}\Delta t = -\lambda \pm \sqrt{\lambda^2 + k^2\Delta x^2}. \tag{50}$$

This shift in frequency makes the upper branch pass through $\omega = 0$ when $k = 0$. For $\lambda = 1/2$, the dispersion relation of the Du Fort–Frankel scheme is close to that of the shifted Klein–Gordon equation, except where $k\Delta x$ approaches $\pm\pi$. The discrepancy in the lower branches at $k = 0$, which is visible for $\lambda = 1/2$ and large for $\lambda = 2$, may be removed by changing the relation between λ and the mass in the Klein–Gordon equation, as described at the end of Section 4. However, this also changes the curvature of the upper branch of the numerical dispersion relation, so it becomes a less accurate approximation to the dispersion relation of the Schrödinger equation.

4. The Du Fort–Frankel scheme as a discretisation of the Klein–Gordon equation

To move the symmetry in the dispersion relation of the Du Fort–Frankel scheme to be around $\omega = 0$, as in the unshifted Klein–Gordon equation, we make the change of variables

$$\psi_j^n = u_j^n e^{in\alpha}. \tag{51}$$

This substitution transforms (46) into an equation with real coefficients:

$$u_j^{n+1} = -u_j^{n-1} + \cos\alpha \left(u_{j+1}^n + u_{j-1}^n\right), \tag{52}$$

which we can rewrite as

$$u_j^{n+1} = -u_j^{n-1} + u_{j+1}^n + u_{j-1}^n - 2\sin^2(\alpha/2)\left(u_{j+1}^n + u_{j-1}^n\right). \tag{53}$$

This coincides with the Ablowitz–Kruskal–Ladik discretisation [21, 22]

$$u_j^{n+1} = -u_j^{n-1} + u_{j+1}^n + u_{j-1}^n - (1/2)\tilde{m}^2\Delta t^2\left(u_{j+1}^n + u_{j-1}^n\right), \tag{54}$$

of the dimensionless one-dimensional Klein–Gordon equation

$$\partial_{tt} u = \partial_{zz} u - \tilde{m}^2 u, \tag{55}$$

with an effective mass $\tilde{m}$ given by

$$\tilde{m}\Delta t = 2\sin(\alpha/2) \sim \alpha\left(1 - \alpha^2/24 + \cdots\right). \tag{56}$$

Thus $\tilde{m}\Delta t \sim \alpha$ for $\alpha \ll 1$, as expected from the small k behaviour of the low frequency branch of the dispersion relation (47) for the Du Fort–Frankel scheme.

The $\tilde{m}$ term in (54) is the natural discretisation of the $\tilde{m}$ term in (55) for the four point stencil in Fig. 1(b). One may instead treat (54) as a discretisation of the Klein–Gordon equation with mass $\tilde{M} = \alpha/\Delta t = (1/\Delta t)\tan^{-1}(m\Delta t)$, with the property that the discrete solutions $\psi_j^n = \exp(\pm in\alpha)$ for wavenumber $k = 0$ have the same frequencies as the continuous solutions $\psi = \exp(\pm i\tilde{M}t)$ of the Klein–Gordon equation. However, the shifted dispersion relation that passes though $\omega = 0$ at $k = 0$ now becomes a less accurate approximation to the dispersion relation of the Schrödinger equation.

5. Leapfrog formulation

The further substitution

$$u_j^n = w_j^n \exp(-in\pi/2) \tag{57}$$

transforms (52) into

$$w_j^{n+1} = w_j^{n-1} + i\cos\alpha\left(w_{j+1}^n + w_{j-1}^n\right). \tag{58}$$

This matches the abstract leapfrog, or second order difference, scheme in (4) for the discrete Hamiltonian $\tilde{\mathsf{H}}$ defined by

$$\left[\tilde{\mathsf{H}}\mathbf{w}^n\right]_j = -\frac{1}{2\Delta t}\cos\alpha\left(w_{j+1}^n + w_{j-1}^n\right) = -\frac{\hbar}{2\hat{m}}\frac{w_{j+1}^n - 2w_j^n + w_{j-1}^n}{\Delta x^2} - \frac{\hbar}{\hat{m}\Delta x^2}w_j^n. \tag{59}$$

The first term is the three-point centred finite difference approximation of the operator $\mathcal{H} = -\hbar/(2\hat{m})\,\partial_{xx}$ with an effective mass

$$\hat{m} = m/\sin\alpha \tag{60}$$

that depends upon α, and hence upon the timestep Δt. The second term in (59) adds a constant potential $V = -\hbar/(\hat{m}\Delta x^2)$ set by the shortest resolved lengthscale Δx. This cancels the contribution from the central point in the three-point Hamiltonian (5), as required to fit the four-point stencil in Fig. 1(b).

The Du Fort–Frankel scheme is thus unitarily equivalent to the leapfrog, or second order difference, scheme for the three-point Hamiltonian (5) and a constant potential. However, the mass in the Hamiltonian is rescaled by $1/(\sin\alpha)$, which diverges as $\Delta t \to 0$. A related result for the leapfrog scheme using the five-point stencil is described in the appendix.

6. Two-time-level formulation

The one-dimensional Klein–Gordon equation can be obtained by eliminating d from the one-dimensional Dirac equation

$$\partial_t u + \partial_z u = md, \tag{61a}$$

$$\partial_t d - \partial_z d = -mu. \tag{61b}$$

Similarly, the discrete equation (52) that determines u at time level $n+1$ in terms of u at the two previous time levels n and $n-1$ can be rewritten as the system

$$u_{j+1}^{n+1} = a u_j^n + b d_j^n, \tag{62a}$$
$$d_{j-1}^{n+1} = a d_j^n - b u_j^n, \tag{62b}$$

relating two variables u and d on the 2 time levels n and $n+1$, with the real coefficients

$$a = \cos\alpha, \quad b = \sin\alpha. \tag{63}$$

A closely related result was used previously to relate the Du Fort–Frankel scheme for the real diffusion equation to some 2-component lattice Boltzmann schemes [23, 24].

The algorithm (62a,b) is equivalent to the composition of two unitary linear operators, streaming S and collisions C, defined by

$$\mathsf{S}\,(u_1, \ldots, u_N, d_1, \ldots d_N)^{\mathsf{T}} = (u_N, u_1, \ldots, u_{N-1}, d_2, \ldots, d_N, d_1)^{\mathsf{T}} \tag{64}$$

for periodic boundary conditions, where $(\cdots)^{\mathsf{T}}$ indicates the (non-Hermitian) transpose of a vector, and

$$\mathsf{C}\begin{pmatrix} u \\ d \end{pmatrix} = \begin{pmatrix} \cos\alpha & \sin\alpha \\ -\sin\alpha & \cos\alpha \end{pmatrix}\begin{pmatrix} u \\ d \end{pmatrix} \tag{65}$$

is applied pointwise to each pair $(u_j^n, d_j^n)^{\mathsf{T}}$. Each operator exactly solves one of the decoupled systems

$$\mathsf{S}\begin{cases} \partial_t u + \partial_z u = 0, \\ \partial_t d - \partial_z d = 0, \end{cases} \qquad \mathsf{C}\begin{cases} \partial_t u = m d, \\ \partial_t d = -m u, \end{cases} \tag{66}$$

over a timestep Δt, so their composition SC defines a discrete unitary evolution that approximates the continuous system (61a,b). This system has arisen before as a quantum lattice gas automaton, a "quantum lattice Boltzmann equation," a quantum generalisation of a random walk on a lattice called the discrete time quantum walk, and as a realisation of the Feynman checkerboard model [22, 25–30]. It can also be derived by integrating the system (61a,b) along its characteristics $x = x_0 \pm (t - t_0)$ for a timestep Δt and applying a unitary change of variables [22, 31].

This discrete system approximates the solution of the continuous system (61a,b) with a local error of $O(\Delta t^2)$, and corresponding global error of $O(\Delta t)$, inherent in the splitting of (61a,b) into two subsystems (66) whose evolutions are given by the non-commuting operators S and C. Moreover, the ordering of the decomposition as SC rather than CS breaks the time-reversal symmetry of the original formulation (52) for u alone across 3 time levels.

Both defects are remedied by the symmetric second-order Strang [32] splitting $\mathsf{C}^{1/2}\mathsf{S}\mathsf{C}^{1/2}$, where $\mathsf{C}^{1/2}$ is a rotation by angle $\alpha/2$ analogous to (65). Writing this out in full gives

$$u_j^{n+1} = \hat{a}\left(\hat{a} u_{j-1}^n + \hat{b} d_{j-1}^n\right) + \hat{b}\left(\hat{a} d_{j+1}^n - \hat{b} u_{j+1}^n\right), \tag{67a}$$
$$d_j^{n+1} = \hat{a}\left(\hat{a} d_{j+1}^n - \hat{b} u_{j+1}^n\right) - \hat{b}\left(\hat{a} u_{j-1}^n + \hat{b} d_{j-1}^n\right), \tag{67b}$$

with $\hat{a} = \cos(\alpha/2)$ and $\hat{b} = \sin(\alpha/2)$. Moreover, by writing the solution after n timesteps as

$$\begin{pmatrix} u_1^n \\ \vdots \\ u_N^n \\ d_1^n \\ \vdots \\ d_N^n \end{pmatrix} = \left(\mathsf{C}^{1/2}\mathsf{S}\mathsf{C}^{1/2}\right)^n \begin{pmatrix} u_1^0 \\ \vdots \\ u_N^0 \\ d_1^0 \\ \vdots \\ d_N^0 \end{pmatrix} = \mathsf{C}^{1/2}\,(\mathsf{S}\mathsf{C})^n\,\mathsf{C}^{-1/2} \begin{pmatrix} u_1^0 \\ \vdots \\ u_N^0 \\ d_1^0 \\ \vdots \\ d_N^0 \end{pmatrix} \tag{68}$$

this symmetric second-order splitting becomes equivalent to the original splitting SC applied to the transformed variables $\tilde{u}_j$ and $\tilde{d}_j$ defined by [22, 33]

$$\begin{pmatrix} \tilde{u}_j^n \\ \tilde{d}_j^n \end{pmatrix} = \mathsf{C}^{-1/2}\begin{pmatrix} u_j^n \\ d_j^n \end{pmatrix}, \tag{69}$$

where $\mathsf{C}^{-1/2}$ is a rotation by angle $-\alpha/2$ applied pointwise to each pair $(u_j^n, d_j^n)^{\mathsf{T}}$.

7. Wu's discrete invariant

The above two-time-level formulations generate a discrete unitary evolution of the u and d variables from time level n to time level $n+1$. They therefore conserve the total probability

$$\mathcal{P}_n = \sum_j \left\{|u_j^n|^2 + |d_j^n|^2\right\} = \sum_j \{|\tilde{u}_j^n|^2 + |\tilde{d}_j^n|^2\}. \tag{70}$$

The two expressions are equal because u_j^n and d_j^n are related to $\tilde{u}_j^n$ and $\tilde{d}_j^n$ by the unitary transformation (69). We can combine (62a,b) to reconstruct

$$d_j^n = \frac{1}{\lambda}\left(u_{j+2}^n - \sqrt{1+\lambda^2}\, u_{j+1}^{n-1}\right) \tag{71}$$

from u at time levels n and $n-1$,and thus write

$$\mathcal{P}_n = \sum_j \left\{ |u_j^n|^2 + \frac{1}{\lambda^2}\left| u_j^n - \sqrt{1+\lambda^2}\, u_{j-1}^{n-1}\right|^2 \right\}. \tag{72}$$

Rewriting this expression using the ψ_j^n variables gives the invariant found by Wu [10]:

$$\mathcal{P}_n = \frac{1}{\lambda^2}\sum_j \left\{ (1+\lambda^2)\left(|\psi_j^n|^2 + |\psi_j^{n-1}|^2\right) - 2\sqrt{1+\lambda^2}\,\mathrm{Re}\left(\psi_j^n\, \overline{\psi_{j-1}^{n-1}}\, e^{-i\alpha}\right)\right\}. \tag{73}$$

Wu [10] called this expression "energy", following common usage for a quadratic invariant of a linear evolution equation in PDE theory. We have shown here that it corresponds to the squared ℓ^2 norm of the solution of the first order system written using u_j^n and d_j^n, which is conserved by unitary evolution. We will find an invariant related to the quantum-mechanical energy, the expectation of the Hamiltonian operator, in the next two sections.

8. Two-time-level schemes in $\psi_\pm$ variables

Having constructed two-time-level schemes in the u and d variables, we can transform them into two-time-level schemes for the $\psi_\pm$ variables. To simplify notation we write $\psi_+(j\Delta x, n\Delta t) = P_j^n$ and $\psi_-(j\Delta x, n\Delta t) = M_j^n$.

Starting from the scheme (61a,b) and applying the unitary transformation

$$u_j^n = \frac{1}{\sqrt{2}}\left(P_j^n + M_j^n\right)e^{-in\alpha}, \quad d_j^n = i\frac{1}{\sqrt{2}}\left(M_j^n - P_j^n\right)e^{-in\alpha}, \tag{74}$$

with a phase rotation to undo the earlier rotation that led to the u and d variables, gives

$$P_j^{n+1} = \frac{1}{2}\left(P_{j+1}^n + P_{j-1}^n\right) + \frac{1}{2}e^{2i\alpha}\left(M_{j-1}^n - M_{j+1}^n\right), \tag{75a}$$

$$M_j^{n+1} = \frac{1}{2}e^{2i\alpha}\left(M_{j+1}^n + M_{j-1}^n\right) + \frac{1}{2}\left(P_{j-1}^n - P_{j+1}^n\right). \tag{75b}$$

This is a unitary, but only first-order accurate, finite difference scheme for the PDE system (31a,b). There is another first-order accurate scheme based on the reversed splitting CS.

Applying the same transformation to the scheme (67a,b) based on the Strang splitting $\mathsf{C}^{1/2}\mathsf{S}\mathsf{C}^{1/2}$ gives

$$P_j^{n+1} = \frac{1}{2}\left(P_{j+1}^n + P_{j-1}^n\right) + \frac{1}{2}e^{i\alpha}\left(M_{j-1}^n - M_{j+1}^n\right), \tag{76a}$$

$$M_j^{n+1} = \frac{1}{2}e^{2i\alpha}\left(M_{j+1}^n + M_{j-1}^n\right) + \frac{1}{2}e^{i\alpha}\left(P_{j-1}^n - P_{j+1}^n\right). \tag{76b}$$

This is a unitary and second-order accurate approximation to the PDE system (31a,b).

For a massless particle with $\alpha = 0$ this is the Lax–Friedrichs [34, 35] scheme for the hyperbolic system $P_t + M_x = 0$, $M_t + P_x = 0$. The usual Lax–Friedrichs truncation error vanishes here because the space and time steps have been synchronised so that the Courant number is unity. This property is more transparent in the earlier u and d variables, for which the various schemes all decouple into $u_j^{n+1} = u_{j-1}^n$ and $d_j^{n+1} = d_{j+1}^n$ for massless particles. These are the exact solutions for propagation of u and d along the light cone characteristics $x = x_0 \pm (t - t_0)$ in $c = 1$ units.

The three variants differ only in the phase of M relative to P, since the matrix C containing the algebraic terms is diagonal in these variables. Eliminating M leads back to the original Du Fort–Frankel scheme for P in the form

$$P_j^{n+1} = -e^{2i\alpha}P_j^{n-1} + \frac{1}{2}\left(1 + e^{2i\alpha}\right)\left(P_{j+1}^n + P_{j-1}^n\right). \tag{77}$$

This is a second-order accurate finite difference approximation to the complex telegraph equation

$$P_{tt} - 2imP_t = P_{xx}. \tag{78}$$

All three variants generate discrete unitary evolution, and thus conserve the total probability

$$\mathcal{P}_n = \sum_j \left\{ |P_j^n|^2 + |M_j^n|^2 \right\}. \tag{79}$$

This expression is invariant under the different phases of M relative to P in the three variants. However, unlike the u and d formulations, there is no local reconstruction of M from P over the three time levels. One would have to solve a tridiagonal system involving $M_{j+1}^n - M_{j-1}^n$, so it is more efficient to solve the pair of equations over two time levels. The advantage of this formulation is that it cleanly separates the Schrödinger-like behaviour in P from the relativistic corrections in M. Only the combined probability (79) is a discrete invariant, but the magnitude of $\sum_j |M_j^n|^2$ gives a measure of the size of the relativistic corrections.

9. A discrete energy invariant

We can construct a second discrete invariant related to the quantum-mechanical energy, the expectation of the Hamiltonian operator [31]. We write the system (76a,b) schematically as

$$\Psi^{n+1} = \mathsf{U}\Psi^n, \tag{80}$$

where U is a unitary discrete-time evolution operator that has no explicit dependence on n. It evolves the wavefunction vector $\Psi^n = (P_1^n, \ldots, P_N^n, M_1^n, \ldots, M_N^n)^\mathsf{T}$ of P and M values on the spatial grid at time level n. We define a complex-valued discrete inner product

$$\langle\Theta|\Phi\rangle = \Delta z \sum_j \overline{\Theta}_j \, \Phi_j, \tag{81}$$

with complex conjugation applied to the first entry. The sum ranges over the $2N$ elements of Ψ^n. This corresponds to treating Θ and Φ as 2-component vectors, and approximating the integral inner product $\int \Theta^\dagger \, \Phi \, dz$ by the trapezoidal rule. The trapezoidal rule is exponentially accurate for domains with equally spaced points and periodic boundary conditions.

The complex-valued matrix element of the evolution operator is then conserved:

$$\langle\mathsf{U}\rangle_{n+1} = \langle\Psi^{n+1}|\mathsf{U}\Psi^{n+1}\rangle = \langle\mathsf{U}\Psi^n|\mathsf{U}\mathsf{U}\Psi^n\rangle = \langle\Psi^n|\mathsf{U}^\dagger\mathsf{U}\mathsf{U}\Psi^n\rangle = \langle\Psi^n|\mathsf{U}\Psi^n\rangle = \langle\mathsf{U}\rangle_n, \tag{82}$$

since $\mathsf{U}^\dagger\mathsf{U} = \mathsf{I}$ is the identity operator as U is unitary. Moreover, U approximates the exact solution operator $\exp(-i\Delta t\mathcal{H})$ for the PDE system (31a,b) with $O(\Delta t^3)$ local error, since (76a,b) is a globally second-order accurate discretisation. Expanding for small Δt gives

$$\langle\mathsf{U}\rangle_n = \langle\Psi^n|\exp(-i\Delta t\mathsf{H})\Psi^n\rangle + O(\Delta t^3) = \langle\Psi^n|\Psi^n\rangle - i\Delta t\langle\Psi^n|\mathsf{H}\Psi^n\rangle - \frac{1}{2}\Delta t^2\langle\Psi^n|\mathsf{H}^2\Psi^n\rangle + O(\Delta t^3). \tag{83}$$

Here H is some discrete Hamiltonian that is compatible with $\mathsf{U} = \exp(-i\Delta t\mathsf{H})$ to within an $O(\Delta t^3)$ error. All of the inner products in the last expression are real, since H is self-adjoint. The imaginary part of $-\langle\mathsf{U}\rangle_n/\Delta t$ is therefore a discrete invariant that approximates $\langle\mathsf{H}\rangle_n$ with an $O(\Delta t^2)$ relative error. The discrete matrix element $\langle\mathsf{U}\rangle_n$ is given concretely by

$$\langle\mathsf{U}\rangle_n = \Delta z \sum_j \left\{\overline{P_j^n}P_j^{n+1} + \overline{M_j^n}M_j^{n+1}\right\}. \tag{84}$$

We can subtract the real quantity $\langle\mathsf{I}\rangle_n = \Delta z \sum_j |P_j^n|^2 + |M_j^n|^2$ to isolate the imaginary part:

$$\begin{aligned}\langle\mathsf{U}-\mathsf{I}\rangle_n = \frac{1}{2}\Delta z \sum_j \Big\{&\overline{P_j^n}\left(P_{j+1}^n - 2P_j^n + P_{j-1}^n\right) + \overline{P_j^n}e^{i\alpha}\left(M_{j-1}^n - M_{j+1}^n\right) \\ &+ \overline{M_j^n}e^{i\alpha}\left(P_{j-1}^n - P_{j+1}^n\right) + \overline{M_j^n}e^{2i\alpha}\left(M_{j+1}^n - 2M_j^n + M_{j-1}^n\right) + 2|M_j^n|^2\left(e^{2i\alpha}-1\right)\Big\},\end{aligned} \tag{85}$$

which rearranges to give

$$\mathrm{Im}\,\langle\mathsf{U}\rangle_n = \cos(\alpha)\Big\{2\sin(\alpha)\Delta z \sum_j \left[|M_j^n|^2 - \frac{1}{2}\,\overline{M_j^n}\left(M_{j+1}^n - 2M_j^n + M_{j-1}^n\right)\right] + \mathrm{Im}\,\Delta z \sum_j \overline{M_j^n}\left(P_{j-1}^n - P_{j+1}^n\right)\Big\}. \tag{86}$$

This concretely defines the discrete H whose matrix element appears in (83). The $|M_j^n|^2$ and $\overline{M_j^n}(P_{j-1}^n - P_{j+1}^n)$ terms are recognisable discrete approximations to terms in (35) for the matrix element of the continuous interaction Hamiltonian $\langle\mathcal{H}_I\rangle$. The replacement of the mass prefactor $2m$ by $2\sin\alpha$, and the extra term involving $M_{j+1}^n - 2M_j^n + M_{j-1}^n$, are needed to create a discrete invariant.

Given this approximation to $\langle\mathcal{H}_I\rangle$, we can use (39) to construct a discrete invariant that approximates the expectation $\mathbb{E}(\mathcal{H}_S)$,

$$\mathcal{E}_n = -\frac{\langle\mathsf{U}\rangle_n/\Delta t}{\|\psi\|^2 + \langle\mathsf{U}\rangle_n/(2m\Delta t)} = \mathbb{E}(\mathcal{H}_S) + O(\Delta t^2). \tag{87}$$

The denominator contains the discrete squared norm $\|\psi\|^2 = \Delta z \sum_j \{|P_j^n|^2 + |M_j^n|^2\}$.

The overall $\cos\alpha$ prefactor in (86) improves the quantitative accuracy of the approximation to $\langle\mathcal{H}_I\rangle$ in the non-relativistic regime, although the difference remains $O(\Delta t^2)$ at fixed mass. To see why, consider

$$P_{j+1}^n - P_{j-1}^n = 2\Delta z\,(\partial_z P)_j^n + O(\Delta z^3) = 4im\Delta z M_j^n + O(\Delta z^3), \tag{88}$$

using the centred finite difference approximation for $\partial_z P$, and then the slowly varying approximation $\partial_z P = 2imM$ from (33), so

$$\mathrm{Im}\sum_j \overline{M_j^n}\left(P_{j-1}^n - P_{j+1}^n\right) = -4\tan(\alpha)\sum_j \left\{|M_j^n|^2 + O(\Delta z^3)\right\}. \tag{89}$$

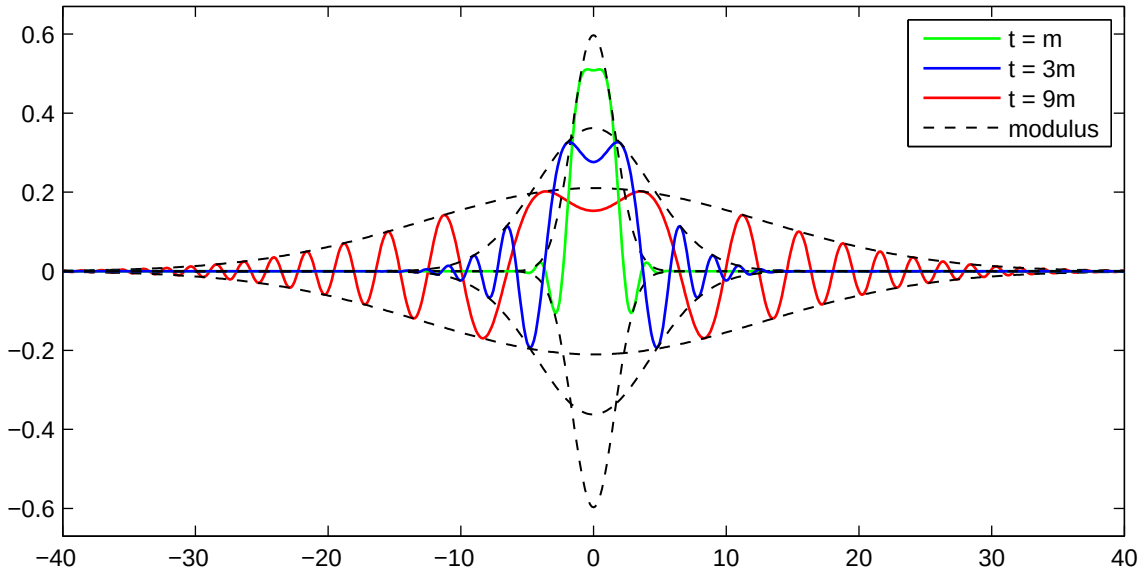

Figure 3: The real part Re ψ (solid lines) and modulus $|\psi|$ (dashed lines) of the solution (93) with $\sigma = 1$ at times $t = m$, $t = 3m$, $t = 9m$.

Combining this expression with the $|M_j^n|^2$ term in (86) gives the leading order approximation

$$\mathrm{Im}\,\langle \mathsf{U} \rangle_n = \cos(\alpha)(2\sin\alpha - 4\tan\alpha)\Delta z \sum_j |M_j^n|^2 + O(\Delta z^3). \tag{90}$$

The improved accuracy follows from the observation that

$$\cos(\alpha)(4\tan\alpha - 2\sin\alpha) = 2m\Delta t + O((m\Delta t)^5), \tag{91}$$

while

$$4\tan\alpha - 2\sin\alpha = 2m\Delta t + O((m\Delta t)^3). \tag{92}$$

10. Numerical experiments

The Gaussian wavepacket

$$\psi(z,t) = (2\sigma/\pi)^{1/4}\,(1 + 2i\sigma t/m)^{-1/2}\exp\left(-\frac{\sigma z^2}{1 + 2i\sigma t/m}\right) \tag{93}$$

is an exact solution of the Schrödinger equation (1) that depends on time only through the ratio $\tau = t/m$, as expected from the structure of (1). Its width grows with time in proportion to $(1 + 4\sigma^2 t^2/m^2)^{1/2}$, as shown in Fig. 3.

Figure 4 shows the discrete ℓ^2 difference between numerical solutions of the centred split form (76a,b) of the du Fort–Frankel scheme and the exact solution (93) at $t = 9m$ for increasing numbers of grid points N. Each simulation was initialised with ψ_+ equal to the solution (93) at $t = 0$, and with ψ_- proportional to the spatial derivative of this solution according to (33). While the differences initially decrease with increasing N, they eventually reach a plateau. Increasing m delays the onset of this plateau to larger N.

By contrast, for each fixed m the numerical solutions of the du Fort–Frankel scheme show the expected second order convergence to reference solutions of the transformed Klein–Gordon system in (31a,b). The reference solutions were obtained by expressing the initial conditions for $\psi_\pm$ as a finite Fourier series. The PDE system (31a,b) then decouples into pairs of ordinary differential equations for each discrete wavenumber k, whose solutions may be expressed using exponentials of 2×2 matrices. In other words, the Hamiltonian becomes purely algebraic, with only 2×2 blocks on the diagonal. This allows an explicit calculation of $\exp(-i(t/\hbar)\mathcal{H})$ in the formal solution (3) of the abstract Schrödinger equation.

Figure 4 confirms that the du Fort–Frankel scheme converges to solutions of the relativistic Klein–Gordon equation, rather than to solutions of the Schrödinger equation. This is exactly analogous to Du Fort & Frankel's observation that solutions of their scheme converge to solutions of a telegraph equation, not to solutions of a diffusion equation [11]. This behaviour is required by the Lax equivalent theorem [35, 36] which states that a consistent finite difference scheme for a well-posed linear initial value problem is convergent if and only if it is stable. The du Fort–Frankel scheme is stable, but does not converge towards solutions of the Schrödinger equation, so it cannot be a consistent finite difference scheme for the Schrödinger equation.

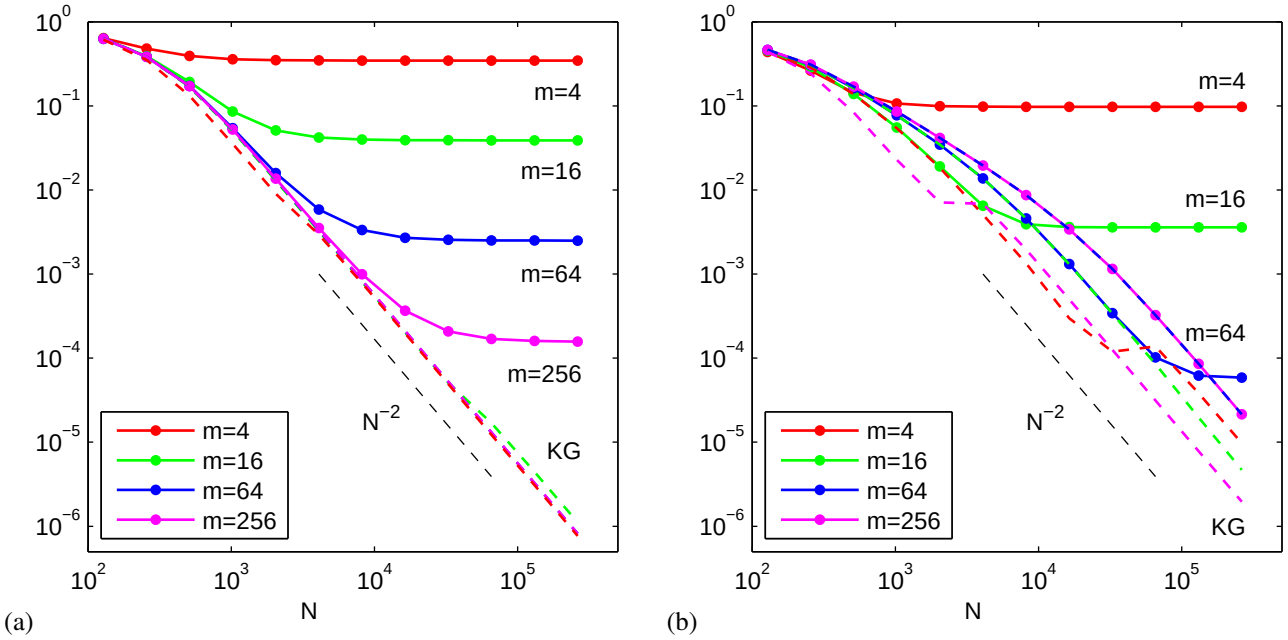

Figure 4: Unsigned differences of the computed (a) ψ_+ and (b) ψ_- from the Schrödinger exact solution (solid lines), and the Klein–Gordon reference solution (dashed lines labelled "KG"), at $t = 9m$ for $m \in \{4, 16, 64, 256\}$ on grids with N points covering $[-64, 64]$.

However, the du Fort–Frankel scheme will converge to solutions of the Schrödinger equation if one rescales both time and the particle mass with increasing resolution N. A more massive particle has a smaller velocity for the same momentum p, or the same characteristic wavenumber $k = p/\hbar$, and is thus less influenced by relativistic effects. The ratio of ψ_- to ψ_+ scales as $p/(mc)$, which becomes smaller as m increases for fixed p.

The difference between the phases of the Schrödinger and Klein–Gordon solutions at time $t = m\tau$ is

$$m\tau\left[\frac{k^2}{2m} - \left(\sqrt{m^2 + k^2} - m\right)\right] \sim \frac{\tau}{8}k^4/m^2. \tag{94}$$

This source of error becomes $O(\Delta t^2)$, the same as the truncation error of the numerical scheme, if we take $m = \mathcal{M}/\Delta t$ for fixed $\mathcal{M}$ and τ. The parameter $\lambda = m\Delta t$ is now fixed as m increases and Δt decreases. However, the du Fort–Frankel dispersion relation (47) gives

$$\omega\Delta t = \cos^{-1}\left(\frac{\cos(k\Delta x)}{\sqrt{1 + \mathcal{M}^2}}\right) - \tan^{-1}\mathcal{M} = \frac{k^2}{2\mathcal{M}}\Delta x^2 + O((k\Delta x)^4). \tag{95}$$

The leading term is the Schrödinger dispersion relation for a particle of mass $\mathcal{M}$, so the scheme is still second-order accurate as $k\Delta x \to 0$, even for $m\Delta t = \mathcal{M}$ fixed. The change in phase over a time $t = m\tau$ is $\omega t = (1/2)\tau k^2 c^2 + O(k^4\Delta t^2)$, which tends to $(1/2)\tau k^2$ as $\Delta t \to 0$ with τ and $c = \Delta x/\Delta t$ fixed.

Figure 5 confirms that this scaling leads to the expected second-order convergence of the numerical solutions for ψ_+ towards the exact solution (93). However, Fig. 6 shows that M_j^n converges to $-i/(2m)\partial_x\psi$ of the exact solution with only first-order accuracy. This lower accuracy can be attributed to the explicit scaling of $-i/(2m)\partial_x\psi$ with $1/m$. Visually indistinguishable results were obtained from the single three-time-level equation (77) by setting P_j^0 and P_j^1 to the exact solution (93) at $t = 0$ and $t = \Delta t$ respectively.

The solution ψ_j^n on space-time points with $j + n$ even is decoupled from the solution on points with $j + n$ odd for any scheme using the four-point stencil in Fig. 1(b). In principle, the solutions on the odd and even sets of points may drift away from each other, but no such artifacts are visible in the wavefunctions in Fig. 3, or in the convergence behaviour. This may be because the different spatial Fourier modes are themselves decoupled in the du Fort–Frankel scheme with periodic boundary conditions, and the initial amplitude of the $(-1)^j$ zig-zag mode is negligibly small.

Figure 7 shows the evolution of the differences between the exact value $\mathbb{E}(\mathcal{H}_S) = 1/(2m)$ and two approximations: the discrete invariant $\mathcal{E}_n$ and the expectation $\mathbb{E}(\mathsf{H}) = \sum_j\{\overline{P_j^n}[\mathsf{H}P]_j^n\}/\sum_j|P_j^n|^2$ of the 3-point discrete Hamiltonian H. These results are from numerical experiments with $m = 4$ and $m = 32$ on grids with 4096, 8192, 16384, 32768, and 65536 points. The oscillations visible in $\mathbb{E}(\mathsf{H})$ have a higher frequency for the $m = 32$ case. Moreover, $\mathbb{E}(\mathsf{H})$ does not converge to $\mathbb{E}(\mathcal{H}_S)$ with increasing resolution at fixed m, due to finite relativistic effects.

The initialisation using (33) eliminates these relativistic effects in $\mathcal{E}_n$. Figure 7(a) shows second-order convergence of $\mathcal{E}_n$ to $\mathbb{E}(\mathcal{H}_S)$ under grid refinement for $m = 4$. However, the convergence behaviour for $m = 32$ shown in Fig. 7(b) is more complicated. The convergence behaviour of $\mathcal{E}_n$ is shown more clearly in Fig. 8, which shows the convergence of $\mathcal{E}_n$ for the discrete initial conditions towards $\mathbb{E}(\mathcal{H}_S)$ under grid refinement for particles with masses ranging from 2 to 64. The

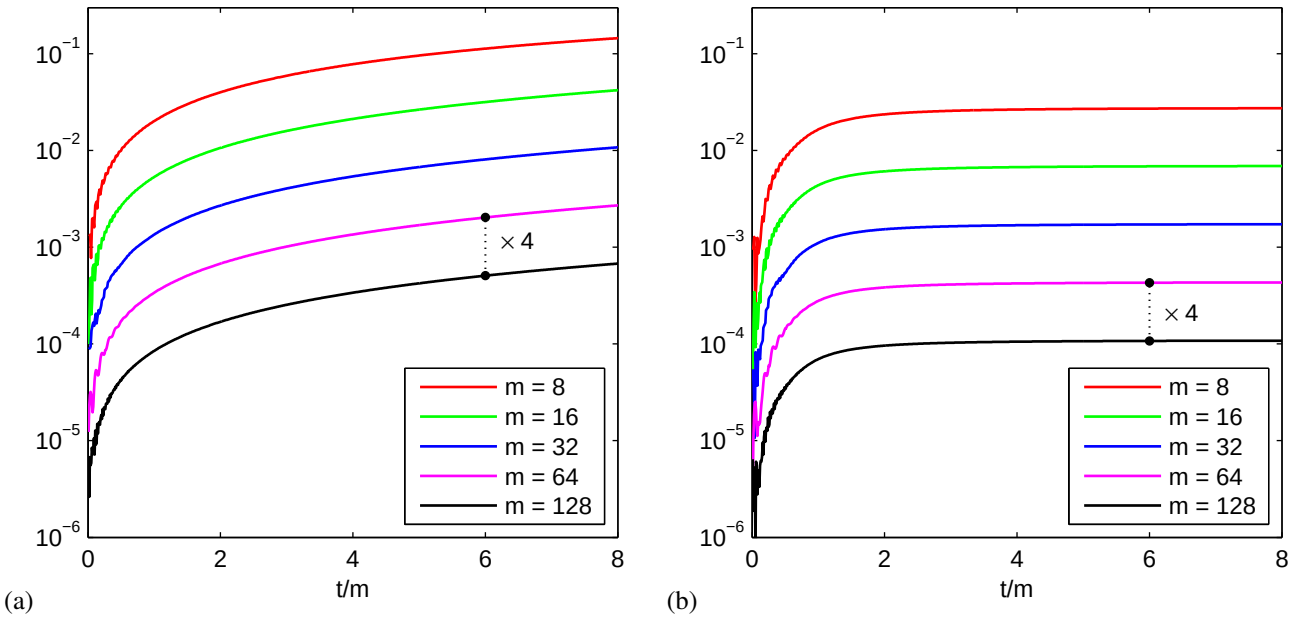

Figure 5: Unsigned differences of the computed (a) ψ_+ and (b) $|\psi_+|$ from the exact solution (93) versus scaled time $\tau = t/m$ for simulations with $m \in \{8, 16, 32, 64, 128\}$ on grids with $256m$ points covering $[-64, 64]$.

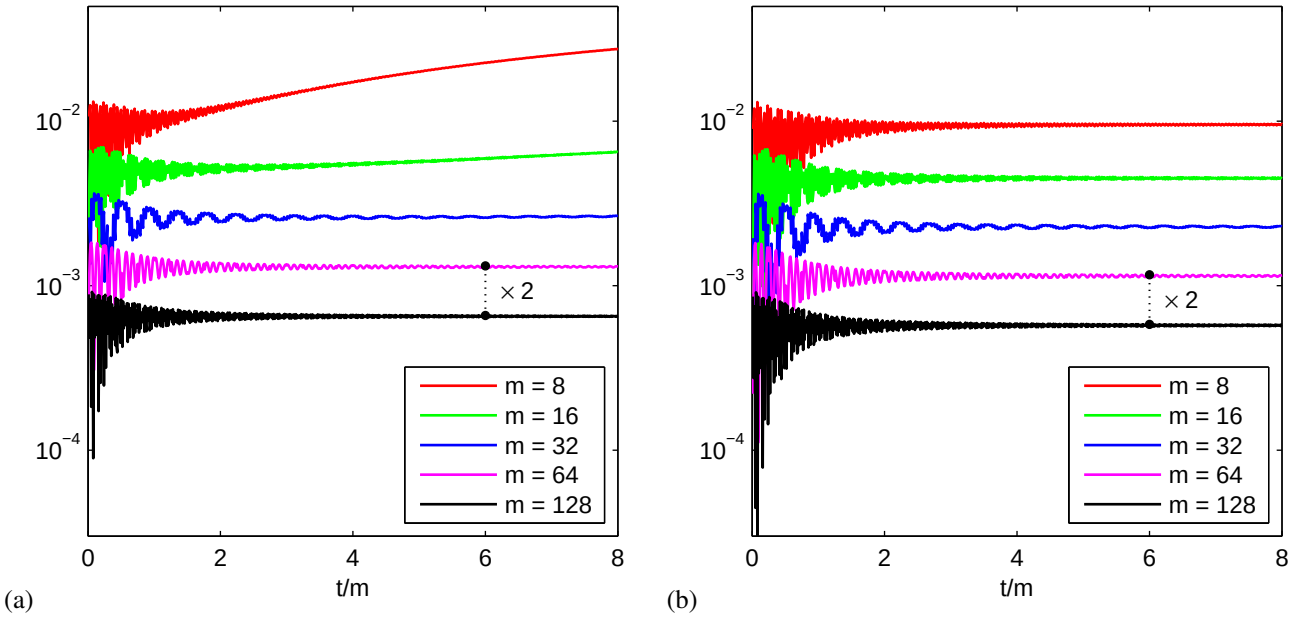

Figure 6: Unsigned differences of the computed (a) ψ_- and (b) $|\psi_-|$ from the scaled derivative of the exact solution (93) versus scaled time $\tau = t/m$ for simulations with $m \in \{8, 16, 32, 64, 128\}$ on grids with $256m$ points covering the interval $[-64, 64]$.

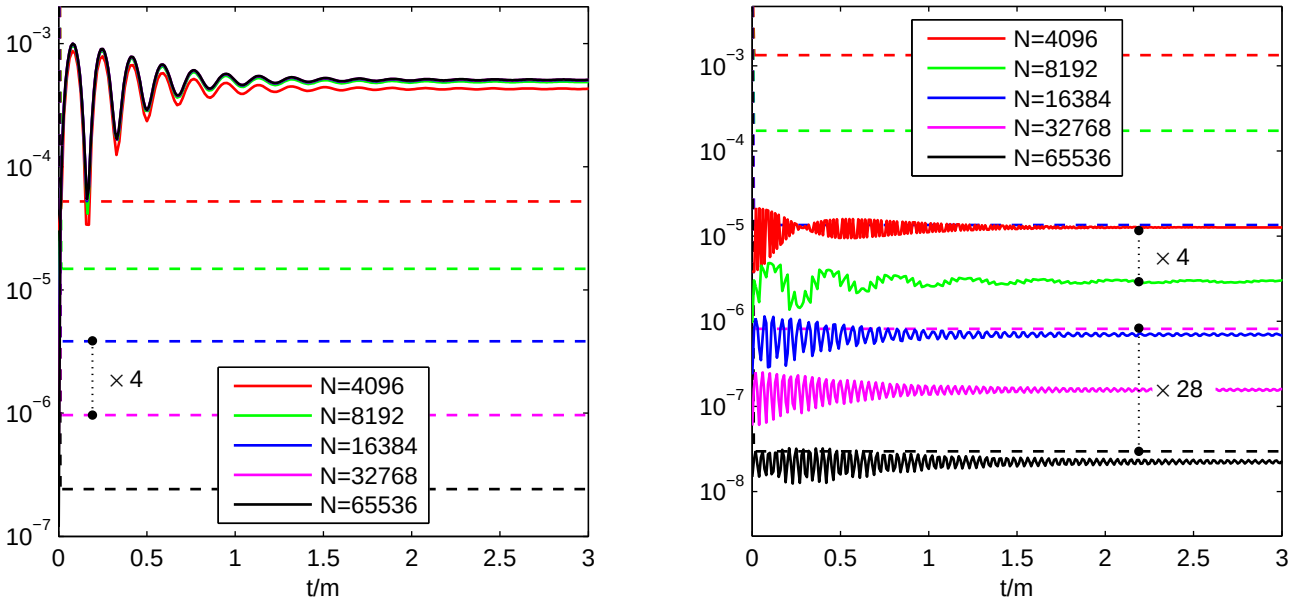

Figure 7: Convergence of the discrete $\mathbb{E}(\mathsf{H})$ (solid lines) and the discrete invariant $\mathcal{E}_n$ (dashed lines) towards $\mathbb{E}(\mathcal{H}_S) = 1/(2m)$ for grids with 4096, 8192, 16384, 32768 and 65536 points. Plot (b) shows data for $m = 32$. Plot (a) shows data for $m = 4$, for which relativistic effects account for the non-convergence of $\mathbb{E}(\mathsf{H})$.

convergence behaviour is simpler without the overall $\cos\alpha$ prefactor in (86), for which the $O(N^{-2})$ asymptotic regime is reached for smaller N. However, the prefactor in the error in the $O(N^{-2})$ asymptotic regime is made significantly smaller by including the $\cos\alpha$ prefactor, as shown by comparing the two plots in Figs. 8(a) and (b).

11. Conclusion

We have shown that the Du Fort–Frankel scheme for the Schrödinger equation for a non-relativistic free particle is equivalent, under a time-dependent unitary transformation, to the Ablowitz–Kruskal–Ladik (AKL) scheme for the Klein–Gordon equation from relativistic quantum mechanics. The AKL scheme is a variational integrator with a discrete action principle [22]. It is stable for $\Delta x = c\Delta t$. It then has the same maximum signal propagation speed c as the Klein–Gordon equation. The conditional convergence of the Du Fort–Frankel scheme to solutions of the Schrödinger equation arises because it is not sufficient to have a converged solution of the Klein–Gordon equation. Solutions of the latter only converge to solutions of the Schrödinger equation in the non-relativistic limit.

The required unitary transformation is a discrete analog of the transformation introduced by Pauli [2] to recover the Schrödinger equation as describing slowly varying solutions of the Klein–Gordon equation in the non-relativistic limit. It is equivalent to a shift in the zero-point of the energy so that the positive energy branch of the Klein–Gordon equation has its minimum energy at zero, rather than at mc^2. We have shown that the same transformation can be motivated using the interaction picture of quantum mechanics, by decomposing the relativistic Hamiltonian into a multiple of the relativistic rest energy, $\mathcal{H}_0 = mc^2\mathsf{I}_2$, and a remainder $\mathcal{H}_I$. Moreover, the matrix element $\langle\mathcal{H}_I\rangle$ coincides with the matrix element $\langle\mathcal{H}_S\rangle$ for the Schrödinger equation when ψ_- is related to ψ_+ by the slowly varying relation (33).

The AKL scheme for the Klein–Gordon equation is in turn unitarily equivalent to the Feynman checkerboard model, to a one-dimensional quantum lattice gas algorithm, to a "quantum lattice Boltzmann equation," and to the one-dimensional discrete time quantum walk [22, 25–30]. These are all discretisations of the one-dimensional Dirac equation, which is a first-order hyperbolic system for a pair of variables u and d, in contrast to the second-order scalar Klein–Gordon equation. These discretisations thus give a unitary evolution of u and d from time level n to time level $n+1$, in contrast to the AKL scheme that determines u at time level $n+1$ in terms of the single variable u at the two preceding times n and $n-1$. This reformulation as a first-order system gives a simple interpretation of the discrete invariant found by Wu [10] as describing conservation of the total probability $\sum_j\{|u_j^n|^2 + |d_j^n|^2\}$ for the two variables in this formulation, not just of $\sum_j |u_j^n|^2$ alone. A further unitary transformation gives a decomposition of the original Du Fort–Frankel scheme into discrete $\psi_\pm$ variables. These lead more easily to the non-relativistic limit, in which $|\psi_-|/|\psi_+| \sim |\mathbf{p}|/mc \ll 1$, than the formulation in the u and d variables that have comparable magnitudes. Any scheme that generates unitary evolution between two time levels through an operator with no explicit time dependence has a second discrete invariant, the matrix element of the evolution operator itself [22]. Expressing this invariant in the discrete $\psi_\pm$ variables, and converting from the normalisation by $\|\psi_+\|^2 + \|\psi_-\|^2$ of the relativistic 2-component wavefunction to the non-relativistic normalisation by $\|\psi_+\|^2$ in the Schrödinger equation, gave a discrete invariant $\mathcal{E}_n$ that approximates the expectation of the non-relativistic Schrödinger Hamiltonian operator $\mathcal{H}_S$.

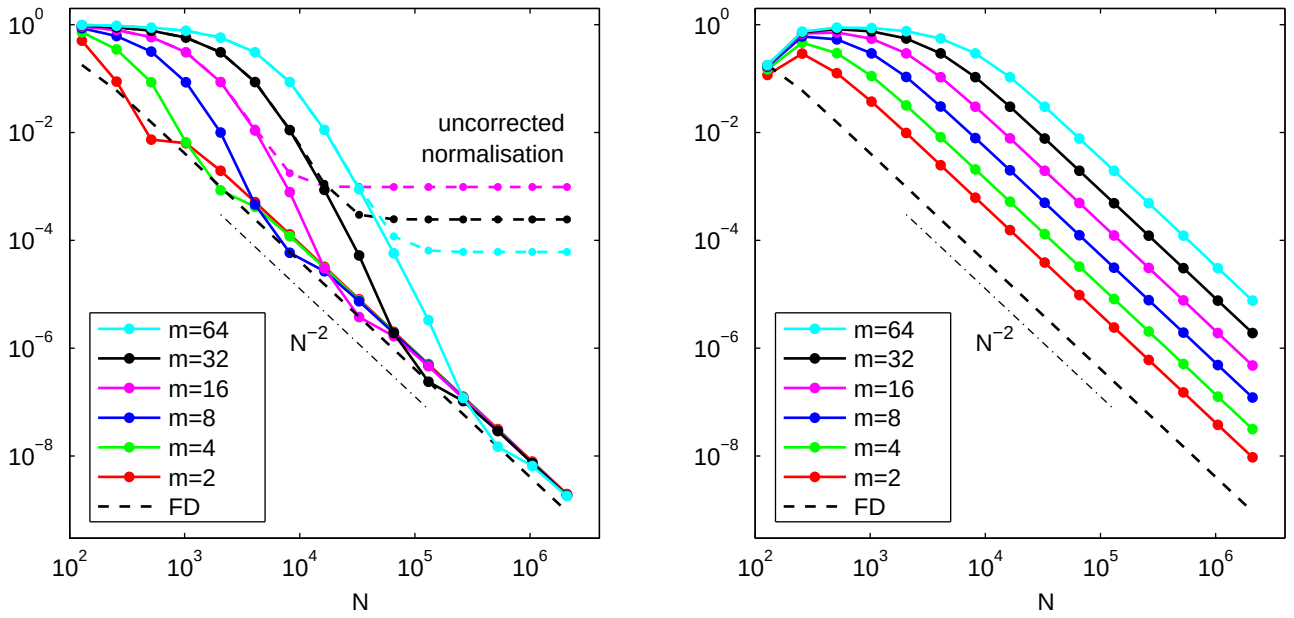

Figure 8: Convergence of the discrete invariant $\mathcal{E}_n$ towards $\mathbb{E}(\mathcal{H}_S) = 1/(2m)$ with increasing number of grid points N for different particle masses $m \in \{2, 4, 8, 16, 32, 64\}$. Plot (a) uses (86) and plot (b) uses (86) without the $\cos\alpha$ prefactor. Plot (a) also shows the errors due to omitting the normalisation correction via (87). The thicker dashed line shows $\mathbb{E}(\mathrm{H})$ for the 3-point finite difference (FD) Hamiltonian (5).

Acknowledgements

The computations employed the Advanced Research Computing facilities at the University of Oxford [37].

A. Appendix. The five-point leapfrog, Harmuth, and Perring–Skyrme schemes

The five-point leapfrog schemes for the Schrödinger and Klein–Gordon equations proposed by Harmuth [5] can similarly be transformed into each other. Consider the five-point leapfrog scheme (6) with an additional constant potential V in the form

$$i\left(\psi_j^{n+1} - \psi_j^{n-1}\right) = -\frac{1}{\lambda}\left(\psi_{j+1}^n - 2\psi_j^n + \psi_{j-1}^n\right) + V\psi_j^n. \tag{96}$$

This scheme uses all five points shown in Fig. 1(b), including the central point ψ_j^n omitted from the schemes discussed in the main text. If we choose the potential $V = M^2\Delta t^2 - 2$, the substitution $\psi_j^n = \exp(i\pi n/2)u_j^n$ transforms (96) into

$$u_j^{n+1} - 2u_j^n + u_j^{n-1} = \frac{1}{\lambda}\left(u_{j+1}^n - 2u_j^n + u_{j-1}^n\right) - M^2\Delta t^2 u_j^n. \tag{97}$$

This is Harmuth's [5] leapfrog scheme for the Klein–Gordon equation with no potential. It is also the linearisation of Perring & Skyrme's [38] scheme for the sine-Gordon equation. The particle mass M and λ are independent parameters in this scheme, with $\lambda = \Delta x^2/(c\Delta t)^2$ instead controlling the ratio of the space and time steps. The dispersion relation for (97) is

$$\sin^2(\omega\Delta t/2) = \frac{1}{\lambda}\sin^2(k\Delta x/2) + \frac{1}{4}M^2\Delta t^2. \tag{98}$$

The scheme is only stable when the right hand side is less than or equal to 1 for all k, which requires $\lambda \geq (1 - M^2\Delta t^2/4)^{-1}$. When $M > 0$ the maximal propagation speed of disturbances in the numerical scheme is thus $\Delta x/\Delta t = c\lambda^{-1/2}$, which is strictly larger than the maximum propagation speed c in the Klein–Gordon equation. For example, Perring & Skyrme [38] ran their simulations with $\Delta x/\Delta t = c/0.95$. By contrast, the Du Fort–Frankel and Ablowitz–Kruskal–Ladik schemes described in the main text are stable with $\Delta x/\Delta t = c$.

References

[1] Bjorken, J.D., Drell, S.D.. Relativistic Quantum Mechanics. New York; London: McGraw–Hill; 1964.

[2] Pauli, W.. General Principles of Quantum Mechanics. Berlin; Heidelberg; New York: Springer; 1980. Translated by P. Achuthan & K. Venkatesan from Pauli's articles in Handbuch der Physik (1933 and 1958).

[3] Schwabl, F.. Advanced Quantum Mechanics. Berlin; London: Springer; 3rd ed.; 2005.

[4] Askar, A., Cakmak, A.S.. Explicit integration method for the time-dependent Schrödinger equation for collision problems. J Chem Phys 1978;68:2794–2798.

[5] Harmuth, H.F.. On the solution of the Schroedinger and the Klein–Gordon equations by digital computers. J Math and Phys 1957;36:269–278.

[6] Kosloff, D., Kosloff, R.. A Fourier method solution for the time dependent Schrödinger equation as a tool in molecular dynamics. J Comput Phys 1983;52:35–53.
[7] Leforestier, C., Bisseling, R.H., Cerjan, C., Feit, M.D., Friesner, R., Guldberg, A., et al. A comparison of different propagation schemes for the time dependent Schrödinger equation. J Comput Phys 1991;94:59–80.
[8] Mazur, J., Rubin, R.J.. Quantum-mechanical calculation of the probability of an exchange reaction for constrained linear encounters. J Chem Phys 1959;31:1395–1412.
[9] Rubin, R.J.. Comment on explicit integration method for the time-dependent Schrödinger equation. J Chem Phys 1979;70:4811–4811.
[10] Wu, L.. Dufort–Frankel-type methods for linear and nonlinear Schrödinger equations. SIAM J Numer Anal 1996;33:1526–1533.
[11] Du Fort, E.C., Frankel, S.P.. Stability conditions in the numerical treatment of parabolic differential equations. Math Tables Other Aids Comput 1953;7:135–152.
[12] Goldberg, A., Schey, H.M., Schwartz, J.L.. Computer-generated motion pictures of one-dimensional quantum-mechanical transmission and reflection phenomena. Amer J Phys 1967;35:177–186.
[13] Crank, J., Nicolson, P.. A practical method for numerical evaluation of solutions of partial differential equations of the heat-conduction type. Math Proc Camb Phil Soc 1947;43:50–67.
[14] Morse, P.M., Feshbach, H.. Methods of Theoretical Physics. New York; London: McGraw–Hill; 1953.
[15] Dellar, P.J.. Macroscopic descriptions of rarefied gases from the elimination of fast variables. Phys Fluids 2007;19:107101–14.
[16] van Kampen, N.G.. Chapman–Enskog as an application of the method for eliminating fast variables. J Statist Phys 1987;46:709–727.
[17] Warn, T., Bokhove, O., Shepherd, T.G., Vallis, G.K.. Rossby number expansions, slaving principles, and balance dynamics. Q J R Meteorol Soc 1995;121:723–739.
[18] Kiefer, C., Singh, T.P.. Quantum gravitational corrections to the functional Schrödinger equation. Phys Rev D 1991;44:1067–1076.
[19] Swartz, B.K.. The construction and comparison of finite difference analogs of some finite element schemes. Tech. Rep. LAUR-74-771; Los Alamos Scientific Laboratory; 1974.
[20] Gottlieb, D., Gustafsson, B.. Generalized Du Fort–Frankel methods for parabolic initial-boundary value problems. SIAM J Numer Anal 1976;13:129–144.
[21] Ablowitz, M., Kruskal, M., Ladik, J.. Solitary wave collisions. SIAM J Appl Math 1979;36:428–437.
[22] Dellar, P.J.. Quantum lattice algorithms: similarities and connections to some classic finite difference algorithms. ESAIM: Proc 2015;52:76–104.
[23] Ancona, M.G.. Fully Lagrangian and lattice Boltzmann methods for solving systems of conservation equations. J Comput Phys 1994;115:107–120.
[24] Dellacherie, S.. Construction and analysis of lattice Boltzmann methods applied to a 1D convection-diffusion equation. Acta Applic Math 2014;131:69–140.
[25] Aharonov, Y., Davidovich, L., Zagury, N.. Quantum random walks. Phys Rev A 1993;48:1687–1690.
[26] Bialynicki-Birula, I.. Weyl, Dirac, and Maxwell equations on a lattice as unitary cellular automata. Phys Rev D 1994;49:6920–6927.
[27] Feynman, R.P., Hibbs, A.R.. Quantum Mechanics and Path Integrals. New York: McGraw–Hill; 1965.
[28] Meyer, D.A.. From quantum cellular automata to quantum lattice gases. J Statist Phys 1996;85:551–574.
[29] Succi, S., Benzi, R.. Lattice Boltzmann equation for quantum mechanics. Physica D 1993;69:327–332.
[30] Yepez, J.. Relativistic path integral as a lattice-based quantum algorithm. Quant Informat Process 2005;4:471–509.
[31] Dellar, P.J.. An exact energy conservation property of the quantum lattice Boltzmann algorithm. Phys Lett A 2011;376:6–13.
[32] Strang, G.. On the construction and comparison of difference schemes. SIAM J Numer Anal 1968;5:506–517.
[33] Dellar, P.J.. An interpretation and derivation of the lattice Boltzmann method using Strang splitting. Comput Math Applic 2013;65:129–141.
[34] Lax, P.D.. Weak solutions of nonlinear hyperbolic equations and their numerical computation. Comm Pure Appl Math 1954;7:159–193.
[35] LeVeque, R.J.. Numerical Methods for Conservation Laws. Basel: Birkhäuser; 1990.
[36] Lax, P.D., Richtmyer, R.D.. Survey of the stability of linear finite difference equations. Comm Pure Appl Math 1956;9:267–293.
[37] Richards, A.. University of Oxford Advanced Research Computing. Technical note doi:10.5281/zenodo.22558; 2015.
[38] Perring, J., Skyrme, T.. A model unified field equation. Nucl Phys 1962;31:550–555.